Korean J. Chem. Eng., 32(11), 2311-2318 (2015)
DOI: 10.1007/s11814-015-0064-4

pISSN: 0256-1115
eISSN: 1975-7220

Mass transfer intensification of nanofluid single drops with effect of temperature

Javad Saien† and Mahdi Zardoshti

Bu-Ali Sina University, 65174, Hamedan, Iran
(*Received 13 January 2015 • accepted 1 April 2015*)

Abstract−The hydrodynamics and mass transfer of organic nanofluid single drops in liquid-liquid extraction process were investigated within temperature range of 20 to 40 °C. Nanofluid drops of toluene+acetic acid, containing surface modified magnetite nanoparticles (NPs) with concentration within the range of (0.0005-0.005) wt%, were conducted in aqueous continuous phase. The rate of solute mass transfer was generally enhanced with NPs until about 0.002 wt%, and small drops benefited more. The enhancement reached 184.1% with 0.002 wt% of NPs at 40 °C; however, adding more NPs led to the mass transfer to either remain constant or face a reduction, depending on the applied temperature. The mass transfer coefficient was nicely reproduced using a developed correlation for enhancement factor of molecular diffusivity as a function of Reynolds and Schmidt numbers.

Keywords: Liquid-liquid Extraction, Nanofluid, Single Drops, Temperature, Mass Transfer Enhancement

INTRODUCTION

Liquid-liquid extraction has found wide applications in different industries such as metal extraction, petroleum refining, nuclear fuel processing, biotechnology and pharmaceutical processing. Mass transfer intensification in this process is affordable economically due to lower operating costs and better performance. Previous works, in this regard, include mainly altering and optimizing influencing parameters such as aqueous phase pH [1,2], temperature [3-5], addition of salts [6,7] and nanoparticles [8-12].

Among these operating parameters, temperature is conventionally used for different process intensifications and is crucial for physical properties alteration. Recently, the influence of temperature on mass transfer of single drops was investigated, and considerable enhancement was demonstrated for different chemical systems when temperature was increased from 15 to 40 °C [3-5].

On the other hand, growing attention has been paid to nanofluid applications in transport phenomena, albeit more in the field of heat transfer. The endeavors for using vast variety of nanoparticles (NPs) in this field have demonstrated higher performance, more energy efficiency and less operating costs.

Investigations on mass transfer of nanofluids were initiated in the first decade of the 21 century. Because of high potential of augmenting in mass transfer processes, the attractive capabilities have attracted the interest of researchers to use nanofluids in this field. The relevant works fall into two main groups of diffusive and convective transports. Diffusive mass transfer occurs for a solute due to concentration gradient in a mixture; however, convective mass transfer refers to a situation where fluid flows and a major part of transport is corresponding to the bulk fluid motion. Most investigations on nanofluids mass transfer have been concerned with the second group. Ashrafmansouri and Nasr Esfahany have recently reported a comprehensive literature review on mass transfer in nanofluids [13]. Amazing results on mass transfer enhancement have been reported, especially in gas-liquid systems [14,15]. Generally, the values of observed enhancements in the rate of mass transfer with nanofluids are much greater than those in heat transfer [13].

In the field of liquid–liquid extraction process, few investigations have been performed. Bahmanyar et al. [10,11], for instance, used silica NPs in kerosene dispersed phase in contact with water continuous phase and using a pulsed liquid-liquid extraction column. The same NP was also used by Asadabadi et al. [12] for the hydrodynamic study of toluene/water chemical system in a horizontal mixer-settler, indicating that introducing NP can reduce the mean drop size with effect of interfacial tension variations. The effect of this NP on phase inversion of liquid-liquid dispersions in a stirred vessel has also been reported [16]. The studied systems for these two earlier works were toluene dispersed in water and vice versa. As a more fundamental approach, mass transfer from nanofluid single drops with magnetite (Fe_3O_4) and alumina (Al_2O_3) NPs has recently been investigated [8]. The effect of NPs on the overall mass transfer coefficient was raised to an average extent of about 72% using 0.002 wt% of NPs, and then a decrease in mass transfer was observed after this optimal concentration. Hence, temperature can potentially affect the function of NPs due to particle motion and the physical property variations. Brownian motion, as a definite function of temperature, can play the main role for this case.

Based on the above background, the aim of this research was to study how the effect of NPs in organic nanofluids can be intensified by temperature within its conventional range and also to find the optimum conditions as most as possible. Magnetite NP was used with the advantage of low price as well as ease of separation. For the aim of design or simulation utilization, the provided data were precisely correlated in terms of most corresponding parameters.

†To whom correspondence should be addressed.
E-mail: saien@basu.ac.ir, jsaien@yahoo.com

EXPERIMENTAL

1. Materials

The frequently used chemical system of toluene-acetic acid-water was employed. It has a high interfacial tension. Toluene and acetic acid are Merck products (≥99.9%) and fresh deionized water of high quality was used as the continuous phase. Modified magnetite, Fe_3O_4, NPs were used to be added in the organic phase as the base fluid. To synthesize this product, ferric chloride anhydrous (≥0.98), ferrous chloride tetrahydrate (≥0.99), ammonium hydroxide (25% NH_3) and oleic acid (ultrapure) were all purchased from Merck. The analysis of collected samples containing acetic acid solute was performed by simple titration method using 0.1 M sodium hydroxide titrant (Merck).

2. Synthesis of Coated Magnetite NPs and Preparation of Nanofluids

The magnetite NPs were produced by co-precipitation from an aqueous Fe^{3+}/Fe^{2+} solution, using concentrated ammonium hydroxide in excess according to the procedure introduced by Ramirez and Landfester [17]. The surface of oxide NPs is hydrophilic and incompatible with nonpolar organic liquids. For dispersion in organic nonpolar dispersed phase, it is therefore necessary to stabilize such NPs for use in organic phase. The coated magnetite NPs was therefore attained by attaching long-chain structure, oleic acid, to the surface of magnetite NPs. The procedure in detail is described in [8].

Fig. 1 shows TEM images of the modified magnetite NPs. An average 12 nm size is relevant. On the other hand, though the provided XRD pattern of modified magnetite NPs agrees with those in a previous report [18], still the particle diameter calculated by Scherrer's equation from the XRD pattern is 10 nm. Different average particle sizes have been reported in previous works, using these methods [19].

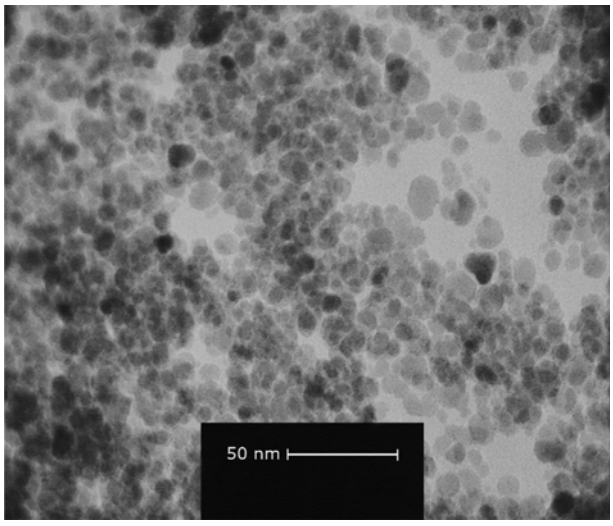

Fig. 1. TEM image of modified magnetite NPs.

The FT-IR spectra of Fe_3O_4 particles, modified with oleic acid as well as bare Fe_3O_4 were also obtained. Compared with the spectrum of the bare Fe_3O_4, five new bands at 1,408.9, 1,437, 1,521, 2,850, and 2,920 cm^{-1} appeared in the spectrum of modified Fe_3O_4. These correspond to the CH_3 umbrella mode of oleic acid, the asymmetric ($-COO^-$) and symmetric ($-COO^-$) stretch vibration bands and symmetric and asymmetric CH_2 stretches of oleic acid, respectively [20].

The two-step nanofluid preparation method was used, as it works well for oxide nano-powders [21]. In this method, the prepared NPs are first dispersed in toluene. The nanofluids are then sonicated to break up any potential clusters of NPs. The concentration of NPs were 0.0005, 0.001, 0.002, 0.003, 0.004 and 0.005 wt% (the uncertainty for NP weight fraction values was $\pm 5\times10^{-6}$).

Nanofluids may face a lack of stability due to NPs precipitation. The suspension stability was therefore evaluated by monitoring the change of sample UV absorbance [16] (at λ=302 nm) with time. Relative absorbance with respect to immediate prepared nanofluid decreased only about 2% after 30 min and about 9% after 120 min, indicating high stability of nanofluids. Of course, the use of nanofluids did not exceed 30 min after just their preparation and the residence time of drops in the column was less than only 5 s.

3. Physical Properties

The ranges of physical properties of the chemical system are listed in Table 1. The average concentration of acetic acid in initial and final points of measurements was 9.2 $g\cdot L^{-1}$; so, in all physical properties determination, this amount was used. Molecular diffusivity in toluene (D_d) was calculated from the Wilke and Chang correlation [22]. To determine the interfacial tension (γ) the drop weight method was used [23,24]. The uncertainty for the interfacial tension measurements was ±0.1 $mN\cdot m^{-1}$. The presence of NPs, within the used concentration range, does not change the interfacial tension significantly; but as illustrated in Fig. 2, this property decreases significantly with temperature. A Ubbleohde viscometer with an uncertainty of $\pm 2\times10^{-3}$ mPa·s was used. The equation for viscosity, according to Poiseuille's law, is:

$$\mu = \rho\left(kt - \frac{c}{t}\right) \quad (1)$$

where μ, ρ and t are viscosity, density and efflux time, respectively, and k and c are the viscometer constants. A calibrated Anton Parr DMA 4500 instrument, provided with automatic viscosity correction, was used to measure the density of liquids. The uncertainty for density measurements was ±0.01 $kg\cdot m^{-3}$, corresponding to a temperature adjustment uncertainty of ±0.01 °C. The k and c param-

Table 1. The ranges of physical properties of the chemical system

Phase	ρ ($kg\cdot m^{-3}$)	μ (mPa·s)	D_d ($m^2\cdot s^{-1}$)[a]	γ ($mN\cdot m^{-1}$)
Dispersed	848.2-867.3 (±0.1)	0.458-0.597 (±0.002)	$[2.82\text{-}3.86]\times10^{-9}$	28.7-32.5 (±0.1)
Continuous	992.1-998.2 (±0.1)	0.658-1.002 (±0.002)		

[a]Molecular diffusivity from the Wilke and Chang correlation [21]

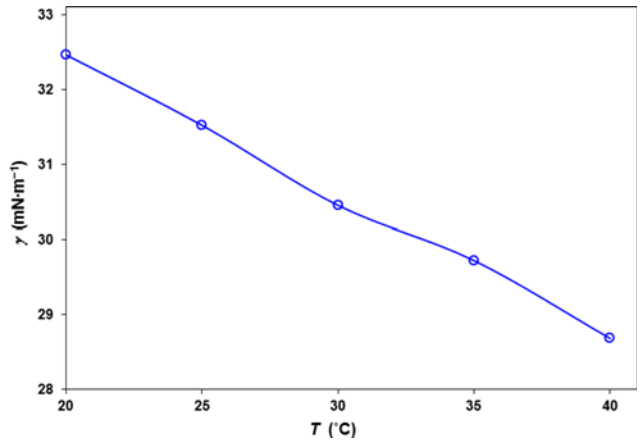

Fig. 2. Variation of interfacial tension of toluene and water with temperature without NPs.

eters were obtained by measurements on frequently used deionized water and benzene. To obtain the density of nanofluids, the equation for suspensions of nanofluids was used [25]:

$$\rho_{nf}=(1-\varphi)\rho_{bf}+\varphi\rho_p \tag{2}$$

where ρ_{nf} is the density of the nanofluid, φ the particle volume concentration, ρ_p the density of the particles (5160.1 kg·m^{-3}) [17] and ρ_{bf} the density of the base fluid (toluene). The volume fraction (φ) can be calculated from

$$\varphi=\left[\frac{\omega_p\rho_{bf}}{(\omega_p\rho_{bf})+\rho_p(1-\omega_p)}\right] \tag{3}$$

where ω_p is the weight fraction of particles. The variation of liquid viscosity with temperature is presented in Fig. 3. The nanofluid viscosity increases very little within the used low dosages of NPs.

4. Experimental Setup and Procedure

The experimental setup has been described in our previous works [4,5]. A jacketed and corrugated wall Pyrex glass column was used as the contactor (Fig. 4). Different drop size formation was provided using nozzles with different tip diameters. The nanofluid was held in a glass syringe and was flowed through a glass nozzle

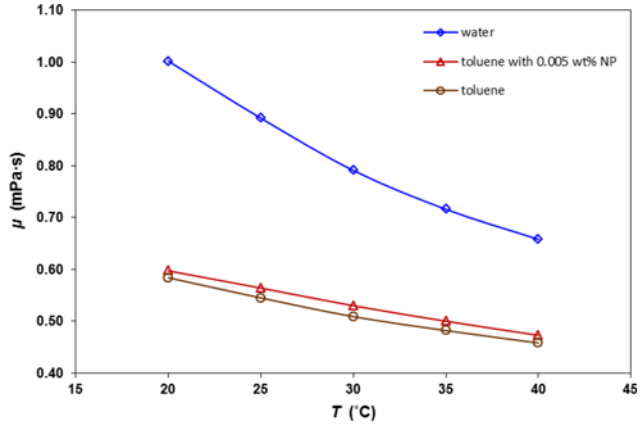

Fig. 3. Variation of water and toluene viscosities with temperature.

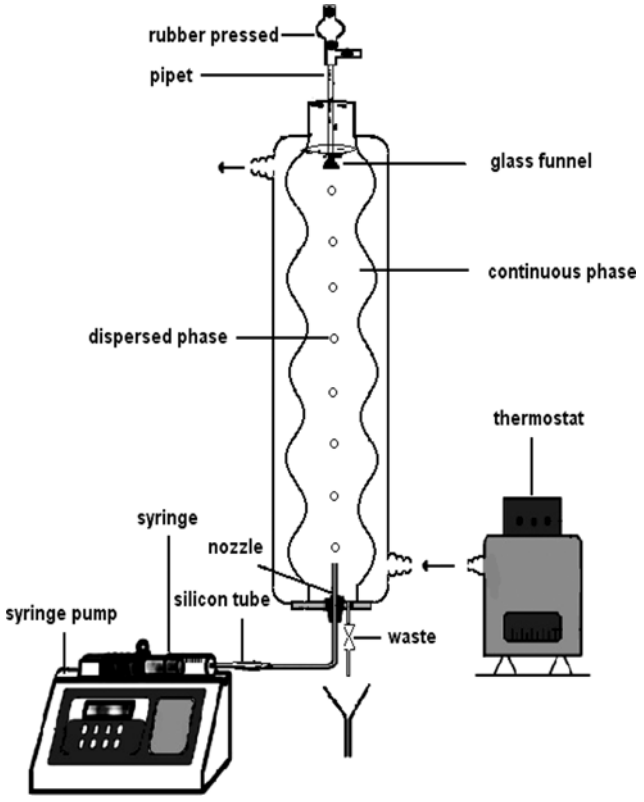

Fig. 4. Details of experimental setup.

into the bottom of the column by means of an adjustable syringe pump (JMS SP-500). The column containing aqueous phase, and conducting tubes was thermostated at desired temperatures (20, 25, 30, 35, and 40 °C, ±0.1 °C). This was established using an adjustable and calibrated thermostat (Julabo F12, Germany). A small inverted glass funnel connected to a pipet was used to catch samples of about 1 mL of dispersed phase at top of the column with 33 cm distance from the initial point. The interfacial area in the funnel was maintained at the level of the pipet inlet. At least three samples were prepared for each experiment and were immediately analyzed by titration with 0.1 M sodium hydroxide titrant; the average concentration was then considered. To omit the influence of unsteady mass transfer during drop formation and its transient velocity, the initial drop concentration was considered for a location of drops moving, 6.5 cm above the nozzles' tip. This was longer than the observed distance to reach steady movement of drops (about 4 cm). To determine the initial concentrations, a small column was used working with the same nozzles. Drops were collected at the same point of 6.5 cm and under the same conditions and drop sizes as in the main column.

For each run, the initial and final concentrations, drop size, and contact time were obtained. The size of drops was determined by knowing the flow rate and the number of drops counted with specified period. The obtained drop size values had an uncertainty of less than ±0.01 mm. The contact time of each drop from the initial to the collection point was measured several times with a stopwatch (uncertainty of ±0.01 s). The terminal velocity was then calculated from the time required for drops to travel from the initial

Table 2. The ranges of generated drops size by the nozzles

Nozzle no.	1	2	3	4	5
d (mm) (±0.01)	2.51-2.69	2.72-2.94	3.18-3.32	3.37-3.49	3.80-3.93

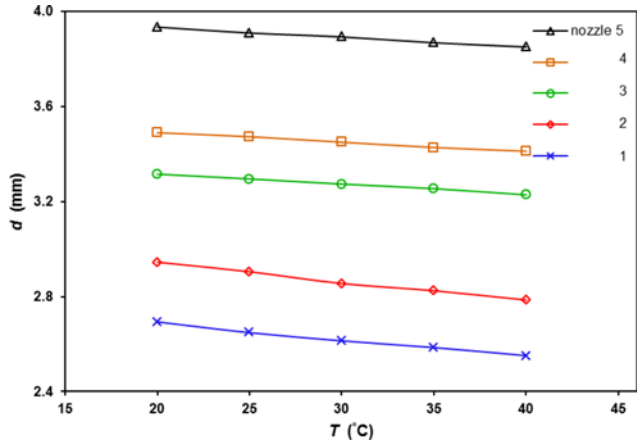

Fig. 5. Variation of generated drop size with temperature for different nozzles and 0.002 wt% of NP concentration.

to the final points. It is notable that no acetic acid adsorption was relevant on NPs due to attached organic long chain oleic acid molecules on their surface.

RESULTS AND DISCUSSION

1. Hydrodynamic Investigations

From previous works, it is clear that the rate of mass transfer is profoundly influenced by drops hydrodynamic factors. The ranges of drop size, generated by nozzles, are given in Table 2. The size of drops decreases mildly with increasing temperature (Fig. 5), mainly due to the decrease of interfacial tension. However, the size of drops does not change much with NP concentration, due to nearly constant interfacial tension and other physical properties.

Drops generated in this work are under circulating conditions. There are a number of criteria in this regard (irrespective of micro-convection, induced by NPs), including the dimensionless group H, defined by Grace et al. [26], Eötvös number and Morton number {$H=(4/3E\ddot{o}M^{-0.149}(\mu_c/\mu_w)^{-0.14}$, $E\ddot{o}=g\Delta\rho d^2/\gamma$ and $M=g\mu_c^4\Delta\rho/\rho_c^2\gamma^3$}, drops Weber number ($We=d u_t^2\rho_c/\gamma$) [27], Reynolds number ($Re=\rho_c u_t d/\mu_c$) [28], the $Re/N_{PG}^{-0.15}$ (N_{PG} is the inverse of the Morton number) [29] and the criterion of critical drop size, d_c, $d>d_c=0.33\mu_c^{0.30}\gamma^{0.43}/(\rho_c^{0.14}\Delta\rho^{0.43})$[30]. In these formulas, u_t is terminal velocity, $\Delta\rho=\rho_c-\rho_d$ and indices c, d and w stand for continuous, dispersed and water cases. As reflected in Table 3, the circulating conditions are dominant.

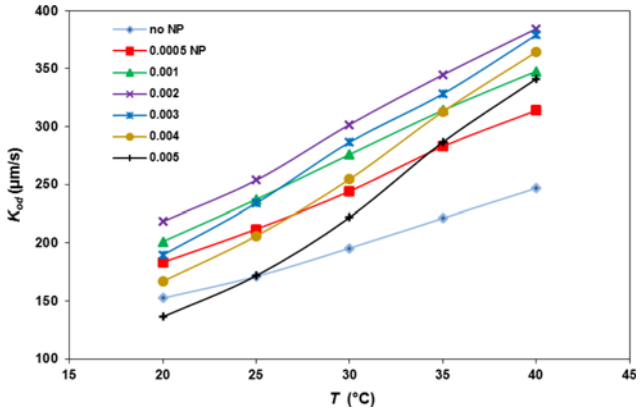

Fig. 6. Variation of overall mass transfer coefficient with temperature for typical nozzle 5.

2. Mass Transfer Investigations

Initiating from a differential mass balance for a drop over a short period time, the overall mass transfer coefficient, K_{od}, can be obtained as:

$$K_{od}=-\frac{d}{6t}\ln(1-E) \quad (4)$$

where t is drops contact time, and E is the extraction fraction, defined by

$$E=\frac{C_{df}-C_{di}}{C_d^*-C_{di}} \quad (5)$$

where C_{di}, C_{df} and C_d^* are initial, final and the equilibrium solute concentrations in drops, respectively. For dispersed to continuous phase mass transfer direction C_d^* is zero since the surrounded continuous phase (3.2 L) was initially pure water and the solute concentration would remain nil even with conducting a high number of drops through the column.

The obtained K_{od} values were within (61.4-384.5) $\mu m\cdot s^{-1}$ for all drop sizes. Uncertainty in the overall mass transfer coefficient values was estimated ± 1.3 $\mu m\cdot s^{-1}$. The average (for different nozzles) K_{od} enhancement with 0.002 wt% concentration of NP at 40 °C was 129.6% (each compared with appropriate drop size without NP) and the enhancement reached to 184.1%, relevant to the smallest drop.

Fig. 6 shows the variation of overall mass transfer coefficient with temperature for a typical used nozzle. As is obvious, significant enhancement is achievable with temperature variation. This matter can be discussed in terms of molecular diffusivity and viscosity. Molecular diffusivity depends directly on the absolute temperature and inversely on the viscosity of solvent [22] that decreases itself with temperature (Fig. 2). The viscosity of organic and aqueous phases decreases with temperature 23.3% and 34.3%, respectively.

Fig. 7 shows the variation of overall mass transfer coefficient

Table 3. Different criteria to indicate circulating conditions of drops

Criterion	2<H<59.3	We<3.58	$Re/(N_{PG}^{0.15})$<20	200<Re<500	$d<d_c$ (mm)
Range in this work	5.61<H<42.6	0.51-1.67	5.78-14.77	235.9-650.2[a]	2.51-3.93<2.69-4.17

[a]Five data with Re>500

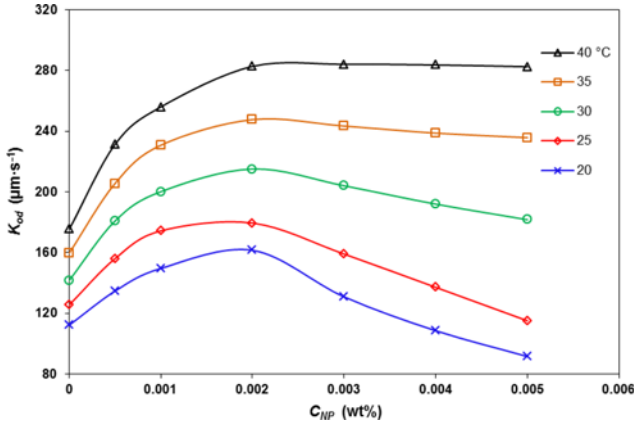

Fig. 7. Overall mass transfer coefficient versus NP concentration, at different temperatures for the typical nozzle 3.

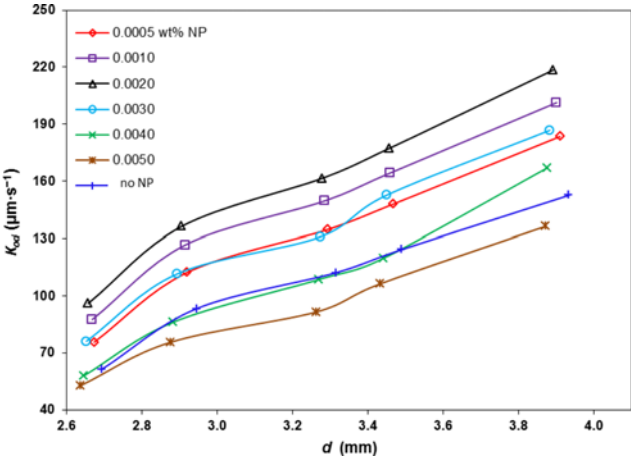

Fig. 8. Variation of overall mass transfer coefficient with drop size at 20 °C.

with NP concentration at different temperatures. At low temperatures used in this work (20, 25 and 30 °C), the maximum K_{od} occurs at 0.002 wt% of NPs and then decreases with extra amounts. Different phenomena have usually been introduced as the dominant mechanisms in nanofluid heat and mass transfer: (i) Brownian motion of NPs and subsequent induced microconvection [31], and (ii) aggregation and clustering. In the field of heat transfer, a number of investigators have reported that Brownian motion of NPs is the main controlling mechanism in the thermal conductivity of nanofluids [32]. It is noteworthy that smaller NPs experience greater motion velocity. According to molecular dynamic simulation, the velocity of a Brownian motion is expressed as [33]:

$$v = \sqrt{\frac{3k_B T}{m_p}} \tag{6}$$

where k_B, T and m_p are the Boltzmann constant, absolute temperature and mass of NP, respectively.

The movement of particles, due to Brownian motion, causes momentum transfer. Thus, the created disturbance field by the motion of NPs, causes microconvection. Considering this liquid flow around moving particles and its possible effect on mass transfer, some researches have proposed that the Brownian motion of particles, by itself, could not contribute directly to the mass transfer enhancement, and the main reason for mass transfer enhancement has been introduced as the microconvection [34,35].

Through molecular dynamics simulations, the influence of NPs properties on the thermal conductivity of nanofluids has been studied with the aim of predicting thermal conductivity enhancement [36,37]. The molecular dynamic simulation results have shown that microconvection enhancement is mainly because the irregular motions of NPs, which leads to increase the intensity of turbulence. The random movements of NPs have been reported, caused by their Brownian motion.

As was pointed out, the rate of mass transfer decreases with NP concentrations more than 0.002 wt%. One possible dominant mechanism here is the particle interaction and facile aggregation [38]. As particles approach each other, the tails of the oleic acid are physically adsorbed on the primary layer by forming an interpenetrating layer of a particle with the tails of the primary layer of an adjacent particle [20]. Increasing the particles' mass because of this aggregation is coincident with the lower microconvection level [39]. A similar variation has been reported for diffusion of rhodamine 6G in water-based alumina nanofluids, and has been attributed to significant interactions among NPs [38].

At higher used temperatures (35 and 40 °C), the enhancing effect of NPs is still observed, until 0.002 wt%; however, after this concentration, K_{od} remains almost constant. This specific behavior can be attributed to the influence of temperature on the degree of aggregation (physically formed). The particle aggregation can be weakened or broken up by heating; so, the Brownian motion of NPs becomes more dominant as temperature rises, and a more efficient microconvection will be relevant. The influence of temperature on NPs has already reported for several cases [40,41].

As Fig. 8 shows, the mass transfer coefficient increases with drop size, due to higher internal circulation or turbulence, and therefore, easier mass transfer per unit time. Meanwhile, larger drops have lower contact time along the column and, thus, higher mass transfer coefficients are relevant. Note that for a specified nozzle, the terminal velocity of the generated drops increases to some extent as temperature increases [3]. Thus, a reduction in contact time is expected. In calculating overall mass transfer coefficient from Eq. (4), contact time reduction with temperature compensates for the slight reduction of generated drops size.

3. Modeling

The simultaneous effects of NPs and temperature on mass transfer can be expressed in terms of involved parameters in the overall mass transfer coefficient. A widely used method is the application of Whitman two-film theory where individual mass transfer coefficients are related via the slope of solute equilibrium curve. Because of very low slope of equilibrium curve within the used concentration range (C_d<2.5 wt%) [42], the continuous phase mass transfer resistance is negligible and $K_{od} \approx k_d$ [28,43].

In an attractive method in modeling, the molecular diffusivity (D_d) in the Newman equation,

$$k_d = \frac{-d}{6t} \ln\left[\frac{6}{\pi^2}\sum_{n=1}^{\infty}\frac{1}{n^2}\exp\frac{-4\pi^2 n^2 D_d t}{d^2}\right] \tag{7}$$

is usually replaced by an overall effective diffusivity, $D_{oe}=\Re D_d$, where $\Re$ is an "enhancement factor" that is based on experimental data and is usually derived from empirical correlations. Effective diffusivity is used to account for internal circulation of droplets. Steiner [44] checked this method on numerous data points and correlated the effective diffusivity with the chemical system properties. Recent works using this method of modeling include prediction of mass transfer coefficient in a regular packed extraction column [45] and in a pulsed packed extraction column [46].

Based on the above approach, each series of experimental results, with relevant hydrodynamic and molecular diffusivity data, were used to determine the corresponding $\Re$ value by fitting to the Eq. (7) accompanied with the effective diffusivity. The obtained $\Re$ values were within the wide range of (2.5-51.1).

With respect to practical design/modeling applications, it was attempted to correlate $\Re$ values. Three influencing parameters are those involved in the rate of mass transfer, i.e., drop size, temperature and NP concentration. Hence, contact time depends on drop size via terminal velocity. Obtaining an equation with these variables can be practically insignificant; however, using relevant dimensionless numbers leads the number of parameters in modeling to be limited. So, the general drops Reynolds number ($Re=\rho_c u_t d/\mu_c$), in terms of the continuous phase physical properties as well as drop hydrodynamic characters (contributing in the extent of circulating inside drops) and the Schmidt number ($Sc=\mu_d/\rho_d D_d$), in terms of the important dispersed phase physical properties were used in modeling. The influence of temperature and NP concentration are involved via the physical properties. The variation of $\Re$ versus these variables are presented in Fig. 9(a) and (b).

Here the mass transfer conventionally used pattern [47], in particular, for enhancement factor as

$$\Re = 1 + a_0 Re^{a_1} Sc^{a_2} \quad (8)$$

was used to correlate the data, where a_0, a_1 and a_2 are the equation parameters (all $\Re$ values are more than unity). However, obtaining just one series of these parameters for 175 provided data points was not consistent because of significant difference among curves presented in Figs. 8 and 9 and subsequently appeared in the corresponding $\Re$ values. So, variations at each NP concentration were considered separately, while the form of equation was maintained. Similarly, in the model proposed by Steiner [44] (for Re<10), an alteration based on using a function of viscosity ratio of phases has been considered.

Eq. (8) was fitted with the relevant Re and Sc data and no correlation was imposed among the parameters considering their sig-

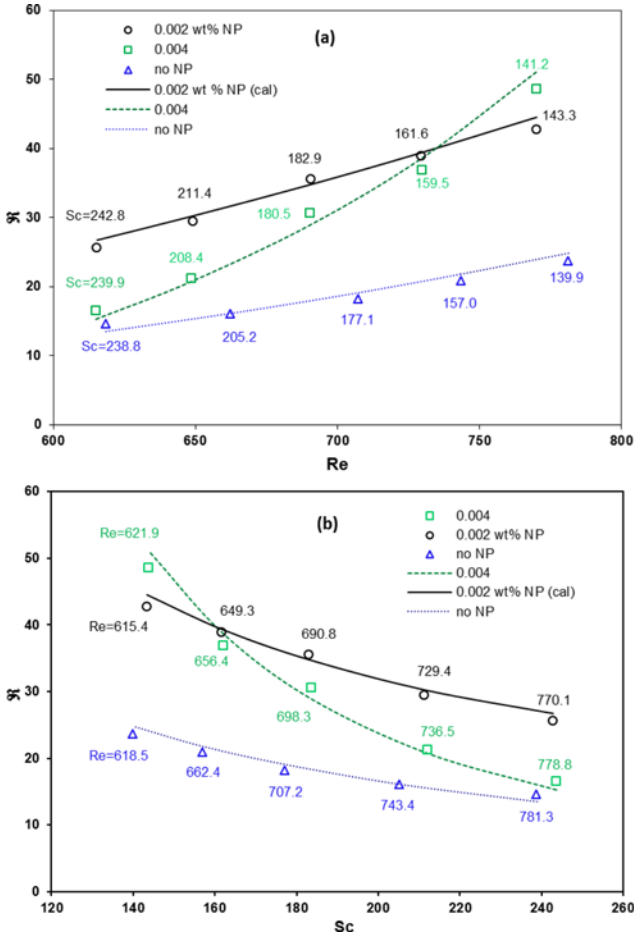

Fig. 9. Variation of $\Re$ with Re (a) and with Sc (b), from 20 to 40 °C for the typical nozzle 5; symbols are experimental data and lines are calculated.

Table 4. Parameters of Eq. (8) and coefficients of determination, R^2

C_{NP} (wt%) ($\pm 5\times10^{-6}$)	a_0	a_1	a_2	R^2
0.0005	0.013	1.608	−0.583	0.931
0.0010	0.030	1.478	−0.554	0.936
0.0020	0.027	1.488	−0.523	0.941
0.0030	0.032	1.802	−0.953	0.959
0.0040	0.074	2.102	−1.499	0.957
0.0050	0.089	2.131	−1.598	0.940

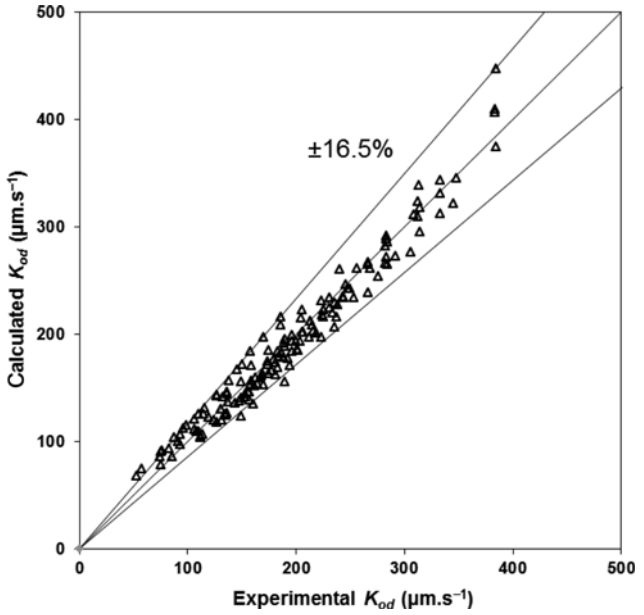

Fig. 10. Comparison between experimental and calculated overall mass transfer coefficients.

nificance. The appropriate obtained values of the parameters, along with the coefficient of determination, R^2, are listed in Table 4. Fig. 9 shows the good proximity of experimental (symbol points) and calculated (continuous lines) $\Re$ values.

Applying the modified Newman equation, accompanied with Eq. (8), gives K_{od} values with a relative deviation of ±16.5% (except five data with more deviations). Fig. 10 shows the agreement between experimental and calculated values, concluding that the proposed model is satisfactory to predict the overall mass transfer coefficient with the simultaneous effect of nanofluid concentration and temperature.

CONCLUSIONS

This work contributes to the understanding of mass transfer in organic nanofluid drops with effect of temperature. In all cases, the mass transfer coefficient increases with temperature; however, the relation between this parameter and nanofluid concentration is not so simple. At low temperatures, the rate of mass transfer first increases and then decreases over the used concentration range of NPs, presumably due to microconvection induced by Brownian motion and particle aggregation, respectively. At the highest used temperature (40 °C) and NP concentrations of 0.002 wt%, the highest rate of mass transfer was achieved. At high temperatures (35 and 40 °C), a plateau trend of variation was observed with high NP concentrations due to the most probable lower aggregation with effect of temperature. The mass transfer coefficient data were nicely reproduced using Newman equation in conjunction with a correlation for enhancement factor as a function of Reynolds and Schmidt numbers.

ACKNOWLEDGEMENT

The authors wish to acknowledge the university authorities for providing the financial support to carry out this work.

NOMENCLATURE

A : absorbance [-]
c : viscometer constant [-]
d : drop diameter [mm]
D : diffusivity [$m^2 \cdot s^{-1}$]
E : extraction fraction [-]
Eö : Eötvös dimensionless number, $g\Delta\rho d^2/\gamma$
g : standard gravity [$m \cdot s^{-2}$]
H : dimensionless group defined by Grace et al. [-]
k : viscometer constant [-]
k_b : Boltzmann constant [m^2 kg s^{-2} K^{-1}]
K_{od} : overall mass transfer coefficient [$\mu m \cdot s^{-1}$]
m : mass of each nanoparticle [kg]
M : Morton dimensionless number, $g\mu_c^4\Delta\rho/\rho_c^2\gamma^3$ [-]
N_{PG} : inverse of Morton dimensionless number [-]
R^2 : coefficient of determination [-]
Re : drop Reynolds number, $\rho_c u_t d/\mu_c$ [-]
Sc : Schmidt number, $\mu_d/\rho_d D_d$ [-]
T : temperature [°C]
t : drops contact time and efflux time in viscometer [s]
u_t : drops terminal velocity [$m \cdot s^{-1}$]
v : root-mean square velocity of a nanoparticle [$m \cdot s^{-1}$]
We : drop Weber number, $\rho_c u_t^2 d/\gamma$ [-]
$\Re$: enhancement factor in diffusivity [-]

Greak Letters

γ : interfacial tension [$mN \cdot m^{-1}$]
Δ : difference [-]
μ : viscosity [$mPa \cdot s^{-1}$]
ρ : density [$kg \cdot m^{-3}$]
φ : particles volume concentration [-]
ω : weight fraction [-]

Subscripts

c : continuous phase
d : dispersed phase
e : effective value
f : final value
i : initial value
o : overall value

Superscript

* : equilibrium

REFERENCES

1. J. Saien and S. Daliri, *Ind. Eng. Chem. Res.*, **47**, 171 (2008).
2. J. Saien and S. Daliri, *Korean J. Chem. Eng.*, **26**(4), 963 (2009).
3. J. Saien and S. Daliri, *Ind. Eng. Chem. Res.*, **51**, 7364 (2012).
4. J. Saien and S. Daliri, *J. Ind. Eng. Chem.*, **20**, 238 (2014).
5. J. Saien and S. Daliri, *J. Taiwan Inst. Chem. Eng.*, **45**, 808 (2014).
6. J. Saien and F. Ashrafi, *Ind. Eng. Chem. Res.*, **48**, 10008 (2009).
7. J. Saien and S. Asadabadi, *J. Taiwan Inst. Chem. Eng.*, **41**, 295 (2010).
8. J. Saien and H. Bamdadi, *Ind. Eng. Chem. Res.*, **51**, 5157 (2012).
9. J. Saien, H. Bamdadi and S. Daliri, *J. Ind. Eng. Chem.*, **21**, 1152 (2015).
10. A. Bahmanyar, N. Khoobi, M. R. Mozdianfard and H. Bahmanyar, *Chem. Eng. Process: Process Intens.*, **50**, 1198 (2011).
11. A. Bahmanyar, N. Khoobi, M. M. A. Moharrer and H. Bahmanyar, *Chem. Eng. Res. Des.*, **92**, 2313 (2014).
12. M. R. Asadabadi, H. Abolghasemi, M. G. Maragheh and P. D. Nasab, *Chem. Eng. Res. Des.*, **91**, 1739 (2013).
13. S. S. Ashrafmansouri and M. Nasr Esfahany, *Int. J. Therm. Sci.*, **82**, 84 (2014).
14. J. K. Lee, J. Koo, H. Hong and Y. T. Kang, *Int. J. Refrig.*, **33**, 269 (2010).
15. B. Olle, S. Bucak, T. C. Holmes, L. Bromberg, A. Hatton and D. I. C. Wang, *Ind. Eng. Chem. Res.*, **45**, 4355 (2006).
16. M. R. Asadabadi, H. Abolghasemi, M. G. Maragheh and P. D. Nasab, *Korean J. Chem. Eng.*, **30**(3), 733 (2013).
17. L. P. Ramirez and K. Landfester, *Macromol. Chem. Phys.*, **204**, 22 (2003).
18. W. Jingjing and L. Dengxin, *Energy Procedia*, **11**, 4794 (2011).
19. S. Komati and A. K.Suresh, *Ind. Eng. Chem. Res.*, **49**, 390 (2009).
20. K. Yang, H. Peng, Y. Wen and N. Li, *Appl. Surf. Sci.*, **256**, 3093

(2010).
21. X. Q. Wang and A. S. Mujumdar, *Int. J. Therm. Sci.*, **46**, 1 (2007).
22. R. B. Bird, W. E. Stewart and E. N. Lightfoot, *Transport Phenomena*, 2nd Ed., Wiley, New York (2007).
23. J. Saien, F. Moghaddamnia and M. Mishi, *Korean J. Chem. Eng.*, **30**(5), 1125 (2013).
24. J. Saien, A. Rezvanipour and S. Asadabadi, *J. Chem. Eng. Data*, **59**, 1835 (2014).
25. B. C. Pak and Y. I. Cho, *Exp. Heat Transfer*, **11**, 151 (1998).
26. J. Grace, T. Wairegi and T. Nguyen, *Chem. Eng. Res. Des.*, **54**, 167 (1976).
27. S. Hu and R. Kinter, *AIChE J.*, **1**, 42 (1955).
28. J. Temos, H. Pratt and G. Steven, *Chem. Eng. Sci.*, **51**, 27 (1996).
29. A. H. P. Skelland, *Interphase mass transfer*, in: *Science and Practice of Liquid-liquid Extraction*, Vol. 1, J. D. Thornton, Ed., Oxford Science Pub., New York (1992).
30. A. J. Klee and R. E. Treybal, *AIChE J.*, **2**, 444 (1956).
31. L. Godson, B. Raja, D. Mohanlal and S. Wongwises, *Renewable Sustainable Energy Rev.*, **14**, 629 (2010).
32. H. Mohammed, A. Al-aswadi, N. Shuaib and R. Saidur, *Renewable Sustainable Energy Rev.*, **15**, 2921 (2011).
33. E. Nagy, T. Feczkoó and B. Koroknai, *Chem. Eng. Sci.*, **62**, 7391 (2007).
34. X. Fang, Y. Xuan and Q. Li, *Appl. Phys. Lett.*, **95**, 203108-1 (2009).
35. S. Krishnamurthy, P. Bhattacharya, P. E. Phelan and R. S. Prasher, *Nano Lett.*, **6**, 419 (2006).
36. W. Cui, Z. Shen, J. Yang and S. Wu, *Appl. Therm. Eng.*, **76**, 261 (2015).
37. W. Cui, M. Bai, J. Lv, L. Zhang, G. Li and M. Xu, *Exp. Therm. Fluid Sci.*, **39**, 148 (2012).
38. J. Veilleux and S. A. Coulombe, *J. Appl. Phys.*, **108**, 104316-1 (2010).
39. C. Wu, T. J. Cho, J. Xu, D. Lee, B. Yang and M. R. Zachariah, *Phys. Rev. E.*, **81**, 011406 (2010).
40. G. Schmid, *Nanoparticles: From Theory to Application*, 2nd Ed. Wiley, Weinheim (2010).
41. S. L. Fiedler, L. Steven, S. Izvekov and A. Violi, *Carbon*, **45**, 1786 (2007).
42. J. Saien, M. Mozafarvandi, S. Daliri and M. Norouzi, *J. Chem. Thermodyn.*, **57**, 76 (2013).
43. J. C. Godfrey and M. J. Slater, *Liquid-liquid Extraction Equipment*, Wiley, Chichester, UK (1994).
44. L. Steiner, *Chem. Eng. Sci.*, **41**, 1979 (1986).
45. A. Rahbar, Z. Azizi, H. Bahmanyar and M. A. Moosavian, *Can. J. Chem. Eng.*, **89**, 508 (2011).
46. M. Torab-Mostaedi and J. Safdari, *Braz. J. Chem. Eng.*, **26**, 685 (2009).
47. R. E. Treybal, Mass Transfer Operations, 3rd Ed. McGraw-Hill, USA (1980).